physica status solidi pss a
www.pss-a.com

Silicon Nanoparticles Prepared by Plasma-Assisted Ablative Synthesis: Physical Properties and Potential Biomedical Applications

Yulia V. Kargina, Aleksandr M. Perepukhov, Aleksandr Yu. Kharin, Elena A. Zvereva, Anatolii V. Koshelev, Sergei V. Zinovyev, Aleksandr V. Maximychev, Alida F. Alykova, Nina V. Sharonova, Vitalii P. Zubov, Mikhail V. Gulyaev, Yurii A. Pirogov, Aleksandr N. Vasiliev, Anatolii A. Ischenko, and Viktor Yu. Timoshenko**

Silicon (Si) nanoparticles (NPs) with small (10^{-3}–10^{-1} at%) content of iron oxide (Fe_2O_3) are prepared by plasma-assisted ablative synthesis. Powders of the prepared Si-iron oxide (SIO) NPs are investigated by means of the transmission electron microscopy, Raman spectroscopy, electron paramagnetic resonance, and magnetic susceptibility measurements. Aqueous suspensions of the NPs are studied by using dynamic light scattering and nuclear magnetic resonance technique. The longitudinal and transverse relaxation times of protons in aqueous suspensions of the NPs are found to be dependent on the iron content. The stronger decrease of the proton relaxation is detected for the samples with higher iron content. Magnetic resonance imaging (MRI) experiments show that SIO NPs have properties of the MRI contrast agent and it is confirmed by in vivo experiments with cancer tumor. Aqueous suspensions of SIO NPs are explored as sensitizers of electromagnetic radio frequency hyperthermia and the highest heating rate is observed for the NPs with smaller hydrodynamic size (≈50 nm). The obtained results indicate possible ways for applications of SIO NPs in the MRI diagnostics and mild therapy of cancer.

1. Introduction

Inorganic nanoparticles (NPs) are promising for both cancer therapy and diagnosis (theranostics) due to their size dependent physical properties. It is known that NPs with sizes less than 100 nm can be used in drug delivery, fluorescent labeling, tissue engineering, tumor detection, and destruction.[1–8] One of the major tasks in biomedicine nowadays is the creation of multimodal NPs, which would allow diagnose tumors at early stages of development and provide combined therapy. Magnetic resonance imaging (MRI) is one of the powerful methods in medical diagnosis. Contrast in the different-modes of MRI can depend mainly on the proton spin density, longitudinal (T_1) and transverse (T_2) relaxation times. In order to enhance quality and

Yu. V. Kargina, Dr. A. Yu. Kharin, Dr. E. A. Zvereva, A.V. Koshelev, Prof. Yu. A. Pirogov, Prof. A. N. Vasiliev, Prof. V. Yu. Timoshenko
Lomonosov Moscow State University
Faculty of Physics
119991 Moscow, Russia
E-mail: juliakargina@gmail.com; timoshen@physics.msu.ru

Yu. V. Kargina, Dr. A. Yu. Kharin, Dr. S. V. Zinovyev, A. F. Alykova, Prof. Yu. A. Pirogov, Prof. V. Yu. Timoshenko
National Research Nuclear University "MEPhI"
Phys-Bio Institute
115409 Moscow, Russia

Dr. A. M. Perepukhov, Prof. A. V. Maximychev
Moscow Institute of Physics and Technology
Dolgoprudny, 141700 Moscow Region, Russia

Dr. E. A. Zvereva, Prof. A. N. Vasiliev
National Research South Ural State University
Chelyabinsk 454080, Russia

A. V. Koshelev
Institute of Experimental Mineralogy
Russian Academy of Sciences (RAS)
142432 Chernogolovka, Moscow Region, Russia

DOI: 10.1002/pssa.201800897

Dr. S. V. Zinovyev
Blokhin National Medical Research Center of Oncology
115478 Moscow, Russia

N. V. Sharonova, Prof. V. P. Zubov, Prof. A. A. Ischenko
Russian Technological University – MIREA
Institute of Fine Chemical Technologies named after M.V. Lomonosov
119454 Moscow, Russia

Dr. M. V. Gulyaev
Lomonosov Moscow State University
Faculty of Fundamental Medicine
117192 Moscow, Russia

Prof. A. N. Vasiliev
National University of Science and Technology "MISiS"
Moscow 119049, Russia

Prof. V. Yu. Timoshenko
Lebedev Physical Institute of the Russian Academy of Sciences
119991 Moscow, Russia

© 2019 WILEY-VCH Verlag GmbH & Co. KGaA, Weinheim

gain more information from the MR images contrast agents (CA) can be administrated into the body. While CAs cannot be visualized directly, they can change relaxation behavior of nearby protons and thus enhance contrast of the images. Usually CAs are paramagnetic metal complexes of gadolinium (III), iron (III), manganese (III).[9]

Gadolinium (Gd) based CAs are widely used. Despite the fact that these CAs have effective contrasting properties safety issues are still open. It was shown that Gd-based CAs can cause allergic reaction, nephrogenic systemic fibrosis, and have long-term accumulation into the brain.[10–12]

Superparamagnetic iron oxide (SPIO) NPs are also strong enhancers of proton relaxation which caused by substantial magnetic field disturbances due to large magnetic moment. SPIO NPs can be used for intestine contrast, liver, spleen, node, and marrow imaging.[13,14] The efficiency of CA can be described by as-called relaxivity, which accounts $r_2 = 100$ $\mathrm{mmol^{-1}\,L\,s^{-1}}$, $r_1 = 30\,\mathrm{mmol^{-1}\,L\,s^{-1}}$ for SPIO NPs. The latter values are much higher than of Gd-based agents $r_2 = 6\,\mathrm{mmol^{-1}\,L\,s^{-1}}$, $r_1 = 4\,\mathrm{mmol^{-1}\,L\,s^{-1}}$.[15] However, it was shown that such NPs may be unsafe for in vivo use.[16] In order to stabilize properties of these nanoparticles several surface coatings have been used.[17]

Radio frequency (RF) induced hyperthermia is efficient noninvasive medical technology development which can be applied to cancer treatment of deep-seated tumors. It was shown that there is heating of tissues under RF radiation and also tumor tissue heat up faster than normal ones.[18] Therefore, it is important to control heat distribution which can be achieved by energy adsorbing agents within the tumors. Solid-state NPs can be used as sensitizers of electromagnetic radiation.[19] Electrically conductive gold NPs provide high absorption of RF radiation which causes Joule heating due to electrical currents in NPs.[20,21] However, it was shown that only 1% of the total dose of administered non-biodegradable gold/silica NPs is accumulating in tumor.[22]

Silicon (Si) NPs are biocompatible and, unlike previous NPs, they can excrete from the body by biodegradation into orthosilicic acid.[23] It was shown that Si NPs can be used as agents for MRI visualization of the tumors,[24,25] as active agents for mild cancer therapy.[26–28]

The effectiveness of Si NPs should be improved in order to allow their application in biomedicine. In this paper nanocomposites mainly based on Si and small content of iron oxide were synthesized by arc-discharge plasma ablative method and were investigated as agent allowing cancer diagnosis, targeted treatment, and monitoring response to the treatment.

2. Experimental Section

2.1. Preparation of NPs

The preparation of SIO NPs was carried out by the arc-discharge plasma ablative method in a closed gas cycle. The system was filled with high purity gas (Ar or N_2) at atmospheric pressure. Purification of the process gas from impurities of moisture and oxygen was carried out with the molten aluminum or special finishing cleaners, irreversibly absorbing impurities to a level of several ppb. A plasma evaporator-condenser operating in an arc low-frequency discharge was used as a reactor. The raw material was Si powder (99.99%) with addition of small (<1%) amount of iron powder (Fe 99.99%), which was injected into the reactor chamber by a gas stream from the corresponding dispenser. In the reactor the powder was evaporated at a temperature of ≈5500 °C. At the exit from the low-temperature plasma zone, the resulting vapor–gas mixture was subjected to cooling gas jets, that is, conditions were created for the condensation of the resulting powder. Then the resulting aerosol with a temperature of 100–200 °C was fed to the refrigerated area, where it was cooled to a temperature of 60–80 °C. Large particles, including the unrefined fraction, were separated from the conditioned ultrafine powder in the classifier of inertial type (for details see ref. [29] and Figure S1, Supporting Information). A schematic view of the arc-discharge plasma ablative synthesis is shown in **Figure 1**.

2.2. Characterization of NPs

Images of SIO NPs were obtained by LEO912 AB OMEGA transmission electron microscope (TEM). Raman spectra were measured by using a DFS-52 spectrometer (LOMO Inc., Russia) under excitation with an Ar^+ laser (Spectra Physics Inc., USA) at 514.5 nm. Average size and potential of a double layer of nanoparticles in suspensions were measured by dynamic light scattering (DLS) method using Malvern Zetasizer Nano ZS. Surface area of NPs was measured by gas absorption BET-method. Electron paramagnetic resonance (EPR) spectra of dried Si-NPs were measured at room temperature by using an EPR spectrometer CMS 8400 ADANI ($f \approx 9.4$ GHz, $B \leq 0.7$ T). The effective $g-$ factors of samples have been calculated with respect to a reference sample of BDPA (a,g-bisdiphenyline-b-phenylallyl) with g-factor 2.00359. To estimate the concentration of paramagnetic centers from EPR data the reference sample of $CuCl_2 \times 2H_2O$ (6×10^{18} spins) has been used. Relaxation times T_1 and T_2 were measured for aqueous suspensions of SIO NPs ($1\,\mathrm{mg\,mL^{-1}}$) by using a Bruker Minispec NMR relaxometer with a 20 MHz probe and magnetic field of 0.5 T at 40 °C. The RF

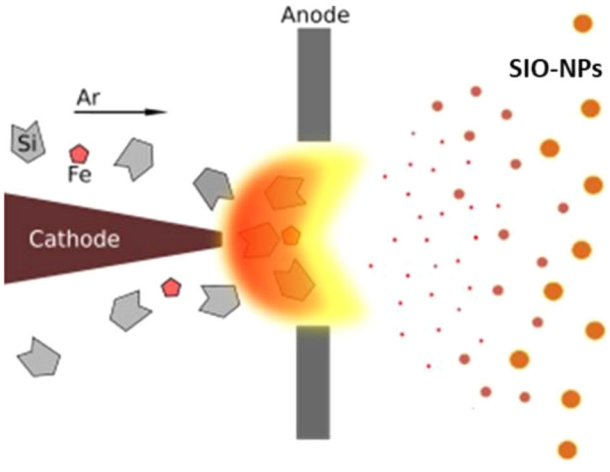

Figure 1. Schematic view of the arc-discharge plasma ablative synthesis used to create SIO NPs.

© 2019 WILEY-VCH Verlag GmbH & Co. KGaA, Weinheim

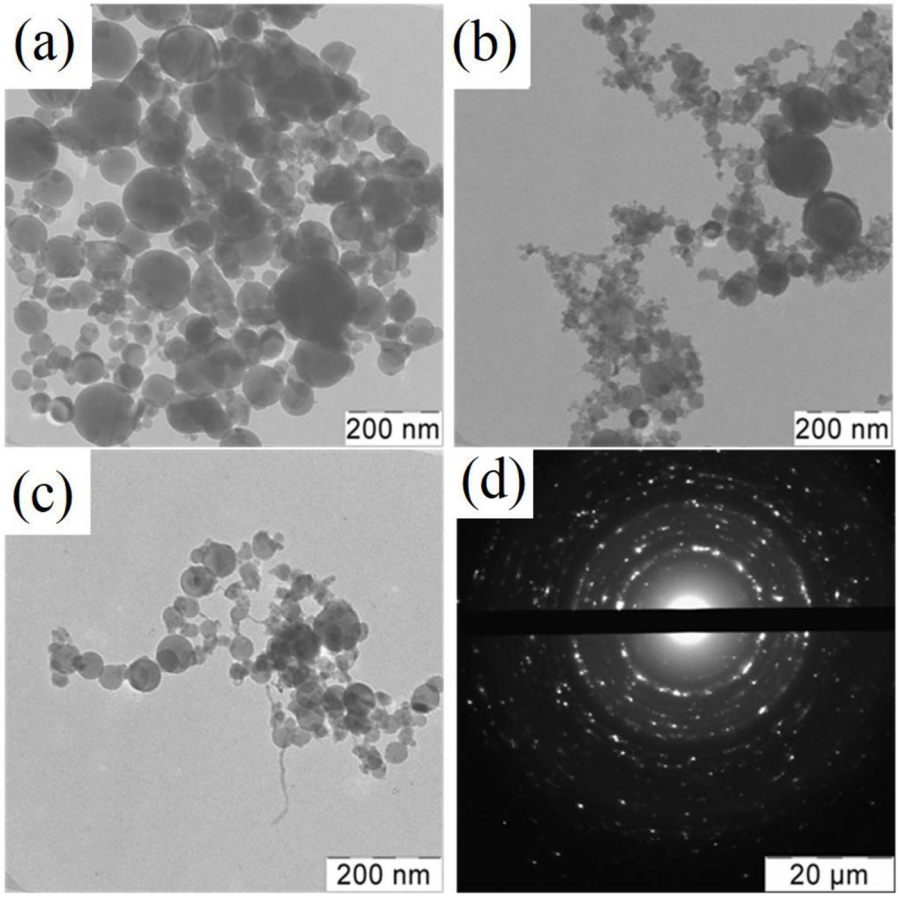

Figure 2. TEM images of SIO NPs with different iron content: (a) 0.004 at%, (b) 0.02 at%, (c) 0.2 at% and (d) typical electron diffraction pattern of SIO NPs.

radiation with frequency of 27 MHz and maximal power of 60 W was provided by a medical device MedTeco-60 (MedTeco Inc., Russia). Aqueous suspensions of SIO NPs with concentration of 0.5 mg mL^{-1} were put into glass bottles (10 mL) and the latter were located between electrodes of the RF device. The RF treatment was done for 2 min. Temperature of the suspension under RF heating was measured using a medical digital precision thermometer TMDP-1 (MIREA, Russia) equipped with EXACON temperature sensor. X-ray diffraction (XRD) study was done by using a RENOM XRD apparatus (Expert Center Ltd., Russia) with Cu Kα line ($\lambda = 0.154184$ nm) at room temperature in air.

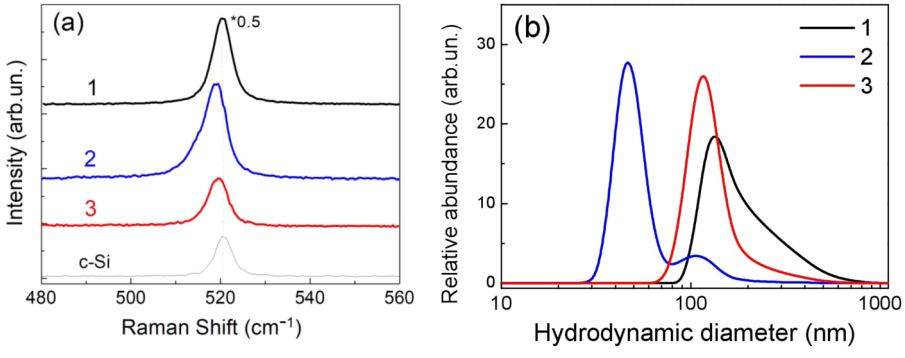

Figure 3. (a) Raman spectra of SIO NPs with different iron content and (b) DLS spectra of their aqueous suspensions, where curves 1, 2, and 3 correspond to the samples with 0.004, 0.02, and 0.2 at% of iron.

© 2019 WILEY-VCH Verlag GmbH & Co. KGaA, Weinheim

Table 1. Investigated samples of SIO NPs and their characteristics.

Sample	Fe content, at. %	Nanocrystal size from XRD, nm	Most probable hydrodynamic size of NPs from DLS, nm	Relaxivity, $L\,g^{-1}s^{-1}$		RF heating rate, $K\,min^{-1}$
				r_1	r_2	
1	0.004	20 ± 5	130	0.05	0.47	6.1
2	0.02	25 ± 5	50	0.13	1.38	12.8
3	0.2	30 ± 5	120	0.83	7.30	1.2

2.3. In Vivo ^{1}MRI Studies

MRI experiments were performed a 7.05 T Bruker BioSpec 70/30 USR MR scanner driven by a ParaVision 5.0 console and equipped with a 105 $mT\,m^{-1}$ gradient amplitude device.

For in vivo ^{1}H MRI studies we used mice of C57BL line with grafted to the right hind paw lung carcinoma (3LL) tumors. All experiments on animals were carried out at animal facilities of the Blokhin National Medical Research Center of Oncology (Moscow, Russia) in accordance with the Principles of Laboratory Animal Care (NIH publication No. 85-23, revised in 1985) and the European Convention for the Protection of Vertebrate Animals used for Experimental and Other Scientific Purposes (Strasbourg, 18.III.1986, revised by the amending protocol ETS 170). The use of experimental animals was approved by Scientific and Ethic committees of the Blokhin National Medical Research Center of Oncology.

Before MRI studies, the animals were anesthetized with 5% isoflurane in the box, and during MRI studies they were subsequently kept in the MR scanner under 1% isoflurane via face mask.

As a transceiver RF coil the proprietary ^{1}H volume coil with an internal diameter of 72 mm was used. The whole body ^{1}H MR images were obtained in the coronal projection using spin echo (SE) pulse sequence with the following scan parameters: field of view: 10×4 cm; matrix: 200×200; repetition time (TR) = 800 ms; echo time (TE) = 14.2 ms; number of slices: 12; slice thickness: 1.5 mm; number of averages: 1; bandwidth: 50 000 Hz; total scan time: 5 min 20 s. Thus, proton density (PD)-weighted MR images were acquired.

The protocol of in vivo MRI studies included the following steps: obtaining whole body PD-weighted MR images before injection the suspension SIO NPs; obtaining whole body PD-weighted MR images 20 min after intratumorally injection of 0.5 mL suspension of SIO NPs (0.5 mg mL^{-1}).

3. Results and Discussion

Figure 2 shows TEM images of SIO NPs. The TEM data reveal almost spherical shape of the NPs and their broad size distributions in the range from 10 to 100 nm. The electron diffraction pattern indicates nanocrystalline structure of the NPs. The crystallinity of SIO NP is also confirmed by XRD measurements (see Figure S4 in Supporting Information). The mean sizes of silicon nanocrystals estimated from the broadening of XRD diffraction line by using the Scherrer equation are given in **Table 1**.

Figure 3a shows Raman spectra of SIO NPs with different iron content. The observed spectra are centered near 521 cm^{-1}, which corresponds to the optical phonons in crystalline Si lattice. The low frequency shoulders and a small (0.5–1 cm^{-1}) shift to lower frequencies of the Raman spectra of SIO NPs compared to the spectrum of c-Si can be explained by a contribution of Si nanocrystals with sized smaller than 10 nm.[26,29]

Figure 3b shows distribution of the hydrodynamic size of SIO NPs dispersed in water. The size distribution possesses the main maxima at 50–120 nm with shoulders at larger sizes. The sample with iron content of 0.02 at% exhibit smallest NPs (50 nm) and additional peak at 100 nm. The latter is obviously related to aggregates of the NPs. Zeta potentials of SIO NPs in aqueous suspensions for all samples is around -20 ± 5 mV, which is typical for Si based NPs.[25–27]

Figure 4 shows EPR spectra of the prepared SIO NP powder with different iron content. EPR signal is overlapping in nature and allows resolving two resonance modes: broad and narrow ones. The dominant broad mode with g-factor ≈2.1 can be related to strongly interacting Fe^{3+} ions in γ-Fe_2O_3 (maghemite).[30–34] The type of iron oxide was also confirmed by temperature measurements of the magnetic susceptibility (see Figure S2, Supporting Information). As one can see from the EPR data all samples contain different amount of iron and estimated content varies from 0.004 at% (sample 1) to 0.2 at% (sample 3). Increasing iron concentration in the samples leads to progressive broadening of the EPR line probably due to

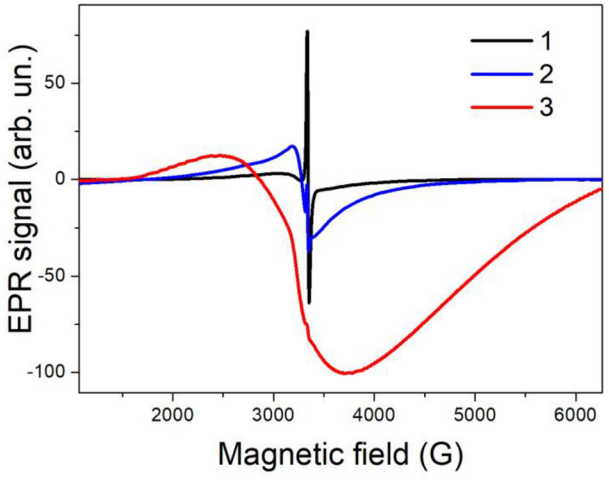

Figure 4. EPR spectra of SIO NP powders with different iron (curves 1, 2, and 3 correspond to the samples with 0.004, 0.02, and 0.2 at% of iron).

© 2019 WILEY-VCH Verlag GmbH & Co. KGaA, Weinheim

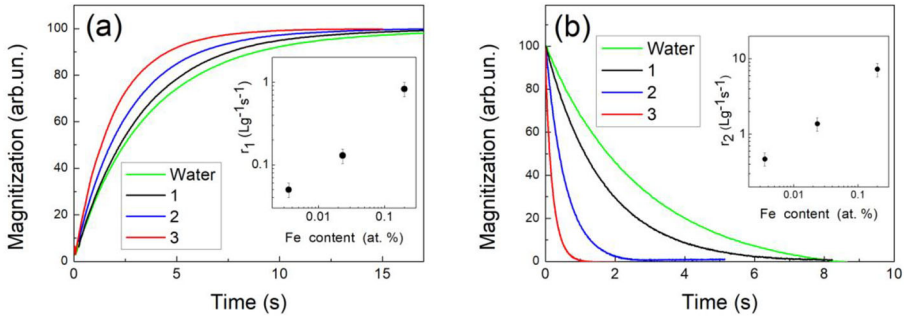

Figure 5. Transients of the proton magnetization: (a) longitudinal and (b) transverse in pure water (green line) and aqueous suspensions of SIO NPs with different iron content (curves 1, 2, and 3 correspond to the samples with 0.004, 0.02, and 0.2 at% of iron). Insets show the corresponding relaxivities vs iron content.

increasing role of spatially inhomogeneous interactions between Fe^{3+} ions. Narrow central mode of the EPR spectrum is characterized by effective *g*-factor of 2.0055 and it can be assigned to Si dangling bonds at the Si/SiO_2 interface.[35,36] The oxidation state of SIO NP surfaces was additionally analyzed by X-ray photoelectron spectroscopy, which revealed the main contribution of SiO_2 surface coating (see Figure S3, Supporting Information).

Figure 5 shows transients of the longitudinal and transverse proton magnetization in suspensions of SIO NPs with different iron content and in pure water (for comparison). The magnetization transients reveal strong shortening for the samples with larger iron concentration. The shortening effect is maximal for the transverse magnetization measurements. To characterize the shortening efficiency one can use the longitudinal and transverse relaxivity, which can be defined as follows[24,25]

$$r_{1,2} = R_{1,2}/C_{NP} \quad (1)$$

where $R_{1,2}$ is the corresponding relaxation rate defined as

$$R_{1,2} = 1/T_{1,2} - 1/T_{1,2}^{w} \quad (2)$$

where C_{NP} is the concentration of SIO NPs, $T_{1,2}$ and $T_{1,2}{}^{w}$ are the relaxation times of SIO NP suspensions and pure water, respectively.

The maximal relaxivity values of $r_1 = 0.8\,L\,g^{-1}\,s^{-1}$ and $r_2 = 7.3\,L\,g^{-1}\,s^{-1}$ are provided by SIO NPs with highest iron content.

Insets in Figure 5 show that both the longitudinal and transverse proton relaxation rates are nearly linear depended on the iron concentration. The higher the iron contents, the higher longitudinal and transverse relaxivities. The transverse relaxivity of SIO NPs with maximal iron content accounts $7.3\,L\,g^{-1}\,s^{-1}$, which corresponds to the molar relaxivity about $200\,mmol^{-1}\,L\,s^{-1}$. The latter value is higher than that for clinically used CAs based on SPIO NPs.[15] The higher relaxivity of SIO NPs can be explained by the contributions of both the iron ions and intrinsic paramagnetic centers (Si dangling bonds).[24,25]

In vivo MRI visualization of mice with grafted tumor was carried out by using SIO NPs with highest relaxivity (sample 3). **Figure 6** shows PD-weighted MR images of the tumor before and after intratumoral injection of SIO NPs. It is seen that tumor area with injected SIO NPs became darker and have more clear boundaries. The MRI study of the mice for time period of 24 h after injection of SIO NPs showed a decrease of the NP induced contrast. This fact can be explained by biodegradation of SIO NPs similarly to that of pure Si NPs.[26,27]

Figure 7 shows time dependent temperature growth of aqueous suspensions of SIO NPs and pure water (for comparison) under RF irradiation. While the heating rate for the sample with highest iron content (curve 3 in Figure 7) was similar to that for pure water ($1\,K\,min^{-1}$), the corresponding

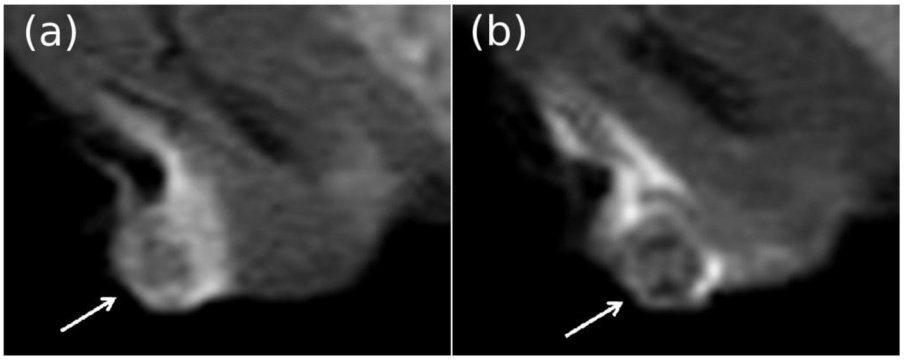

Figure 6. MRI of cancer tumor in mouse (a) before and (b) 20 min after injection of SIO NPs.

© 2019 WILEY-VCH Verlag GmbH & Co. KGaA, Weinheim

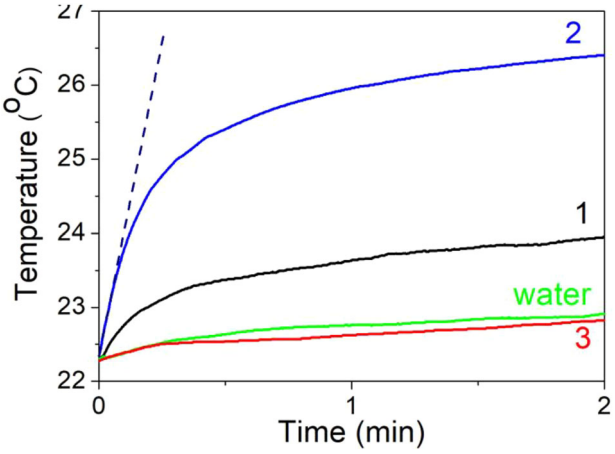

Figure 7. Time dependences of the temperature of SIO NP suspensions (1 mg mL^{-1}) with different iron content (curves 1, 2, and 3 correspond to the samples with 0.004, 0.02, and 0.2 at%) and pure water (green curve) under RF irradiation with frequency 27 MHz and intensity 10 W cm^{-2}.

value for the sample with 0.02 at% of iron approached 13 K min^{-1}. This fact can be explained by smaller size of SIO NPs in aqueous media for the latter sample (see Figure 3b), which influences strongly the RF heating.[26]

4. Conclusions

Crystalline Si NPs with iron content varied from 0.004 to 0.2 at% and mean nanocrystal sizes of 20–30 nm were produced by a scalable plasma ablative method and were investigates as potential contrast agents for MRI and sensitizers for RF hyperthermia. It was found that SIO NPs dispersed in aqueous media significantly affected both the longitudinal and transverse proton relaxations. The maximal longitudinal and transverse relaxivities were obtained for the samples with the highest iron content. The RF-induced heating rate of aqueous suspensions of NPs was maximal for the NPs with smaller hydrodynamic diameter of about 50 nm. The obtained results indicate that SIO NPs with optimized iron content can be promising for applications as MRI contrast agents and sensitizers of the RF-induced hyperthermia of cancer. The optimal size and content of Si/iron oxide nanoparticles to satisfy requirements for the both modalities are subjects of further research.

Supporting Information

Supporting Information is available from the Wiley Online Library or from the author.

Acknowledgments

Authors acknowledge S.S. Abramchuk for the TEM measurements, P.A. Storozhenko and E.K. Dobrinsky for the assistance in nanoparticles synthesis, providing a scheme of the experimental setup and fruitful discussions. The nanoparticle formation and magnetic measurements were partially supported by the Russian Foundation for Basic Research (grants Nos. 16-29-11741 OFI-m and 16-02-00668). Yu.V.K., A.Yu.K., and V.Yu.T. thank the support of their work on the nanoparticle characterization and in vivo experiments by the Russian Science Foundation (grant No. 16-13-10145). A.N.V. acknowledges support by the Ministry of Education and Science of the Russian Federation in the framework of Increase Competitiveness Program of NUST "MISiS" grant K2-2017-084, by acts 211 of the Government of Russian Federation, Contracts No. 02.A03.21.0004 and 02.A03.21.0011.

Conflict of Interest

The authors declare no conflict of interest.

Keywords

hyperthermia, imaging, iron oxide, magnetic resonance, nanoparticles, silicon

Received: November 16, 2018
Revised: January 27, 2019
Published online:

[1] K. Cho, X. Wang, S. Nie, Z. Chen, D. M. Shin, *Clin. Cancer Res.* **2008**, *14*, 1310.
[2] M. Bruchez, M. Moronne, P. Gin, S. Weiss, A. P. Alivisatos, *Science* **1998**, *281*, 2013.
[3] J. Ma, H. Wong, L. B. Kong, K. W. Peng, *Nanotechnology* **2003**, *14*, 619.
[4] A. K. Gupta, M. Gupta, *Biomaterials* **2005**, *26*, 3995.
[5] D. Gerion, F. Pinaud, S. C. Williams, W. J. Parak, D. Zanchet, S. Weiss, A. P. Alivisatos, *J. Phys. Chem. B* **2001**, *105*, 8861.
[6] G. von Maltzahn, J. H. Park, A. Agrawal, N. K. Bandaru, S. K. Das, M. J. Sailor, S. N. Bhatia, *Cancer Res.* **2009**, *69*, 3892.
[7] A. Bitar, N. M. Ahmad, H. Fessi, A. Elaissari, *Drug Discov. Today* **2012**, *17*, 1147.
[8] Z. Li, J. C. Barnes, A. Bosoy, J. F. Stoddart, J. I. Zink, *Chem. Soc. Rev.* **2012**, *41*, 2590.
[9] G. J. Strijkers, W. J. M. Mulder, G. A. F. van Tilborg, K. Nicolay, *Anticancer Agents Med. Chem.* **2007**, *7*, 291.
[10] I. Elbeshlawi, M. S. AbdelBaki, *Pediatr. Neurol.* **2018**, *86*, 27.
[11] H. S. Thomsen, S. K. Morcos, P. Dawson, *Clin. Radiol.* **2006**, *61*, 905.
[12] S. Franckenberg, F. Berger, S. Schaerli, G. Ampanozi, M. Thali, *Radiol. Case Rep.* **2018**, *13*, 299.
[13] J. W. M. Bulte, D. L. Kraitchman, *NMR Biomed.* **2004**, *17*, 484.
[14] C. Xu, S. Sun, *Adv. Drug Deliv. Rev.* **2013**, *65*, 732.
[15] C. W. Jung, P. Jacob, *Magn. Reson. Imaging* **1995**, *13*, 661.
[16] M. Mahmoudi, H. Hofmann, B. Rothen-Rutishauser, A. Petri-Fink, *Chem. Rev.* **2012**, *112*, 2323.
[17] A. Jedlovszky-Hajdú, F. B. Bombelli, M. P. Monopoli, E. Tombácz, K. A. Dawson, *Langmuir* **2012**, *28*, 14983.
[18] J. H. Kim, E. W. Hahn, S. A. Ahmed, *Cancer* **1982**, *50*, 478.
[19] E. S. Day, J. G. Morton, J. L. West, *J. Biomech. Eng.* **2009**, *131*, 074001.
[20] P. Cherukuri, E. S. Glazer, S. A. Curley, *Adv. Drug Deliv. Rev.* **2010**, *62*, 339.
[21] C. J Gannon, C. R. Patra, R. Bhattacharya, P. Mukherjee, S. A Curley, *J. Nanobiotechnol.* **2008**, *6*, 2.
[22] W. D. James, L. R. Hirsch, J. L. West, P. D. O'Neal, J. D. Payne, *J. Radioanal. Nucl. Chem.* **2007**, *271*, 455.
[23] J. H. Park, L. Gu, G. von Maltzahn, E. Ruoslahti, S. N. Bhatia, M. J. Sailor, *Nat. Mater.* **2009**, *8*, 331.

© 2019 WILEY-VCH Verlag GmbH & Co. KGaA, Weinheim

[24] M. B. Gongalsky, Y. V. Kargina, L. A. Osminkina, A. M. Perepukhov, M. V. Gulyaev, A. N. Vasiliev, Y. A. Pirogov, A. V. Maximychev, V. Y. Timoshenko, *Appl. Phys. Lett*. **2015**, *107*, 233702.
[25] Y. V. Kargina, M. B. Gongalsky, A. M. Perepukhov, A. A. Gippius, A. A. Minnekhanov, E. A. Zvereva, A. V. Maximychev, V. Y. Timoshenko, *J. Appl. Phys*. **2018**, *123*, 104302.
[26] K. P. Tamarov, L. A. Osminkina, S. V. Zinovyev, K. A. Maximova, J. V. Kargina, M. B. Gongalsky, Yu. Ryabchikov, A. Al-Kattan, A. P. Sviridov, M. Sentis, A. V. Ivanov, V. N. Nikiforov, A. V. Kabashin, V. Yu Timoshenko, *Sci. Rep*. **2014**, *4*, 7034.
[27] A. P. Sviridov, V. G. Andreev, E. M. Ivanova, L. A. Osminkina, K. P. Tamarov, V. Yu Timoshenko, *Appl. Phys. Lett*. **2013**, *103*, 193110.
[28] V. Y. Timoshenko, A. A. Kudryavtsev, L. A. Osminkina, A. S. Vorontsov, Y. V. Ryabchikov, I. A. Belogorokhov, D. Kovalev, P. K. Kashkarov, *JETP Lett*. **2006**, *83*, 423.
[29] A. A. Ischenko, G. V. Fetisov, L. A. Aslanov, *Nanosilicon: Properties, Synthesis, Applications, Methods of Analysis and Control*. CISP, CRC, Taylor & Francis Group, NY **2014**, p. 714.
[30] Yu. A. Koksharov, D. A. Pankratov, S. P. Gubin, I. D. Kosobudsky, M. Beltran, Y. Khodorkovsky, A. M. Tishin, *J. Appl. Phys*. **2001**, *89*, 2293.
[31] C. Cannas, D. Gatteschi, A. Musinu, G. Piccaluga, C. Sangregorio, *J. Phys. Chem*. **1998**, *102*, 7721.
[32] N. Noginova, F. Chen, T. Weaver, E. P. Giannelis, A. B. Bourlinos, V. A. Atsarkin, *J. Phys. Condens. Matter* **2007**, *19*, 246208.
[33] D. Prodan, V. V. Grecu, M. N. Grecu, E. Tronc, J. P. Jolivet, *Meas. Sci. Technol*. **1999**, *10*, L41.
[34] N. Guskos, G. J. Papadopoulos, V. Likodimos, S. Patapis, D. Yarmis, A. Przepiera, K. Aidinis, *Mater. Res. Bull*. **2002**, *37*, 1051.
[35] C. R. Helms, E. H. Poindexter, *Rep. Prog. Phys*. **1994**, *57*, 191.
[36] R. N. Pereira, D. J. Rowe, R. J. Anthony, U. Kortshagen, *Phys. Rev. B* **2011**, *83*, 155327.

 © 2019 WILEY-VCH Verlag GmbH & Co. KGaA, Weinheim